CHAPTER 3

STUDY ON STRUCTURAL, OPTICAL AND MAGNETIC PROPERTIES OF COBALT DOPED ZINC OXIDE NANOPARTICLES

3.1. INTRODUCTION

The subject of transition metal (TM) doped semiconductors has attracted considerable attention due to its wide applications in optoelectronic devices, solar cell, spintronic devices, flat panel display etc. The dilute magnetic semiconductors materials are interesting because of combination of both semiconducting and magnetic properties within the same materials. Zinc oxide is wide band gap optically transparent semiconductor. It has large excitation binding energy of 60meV and considered as *n*- type material [91-92]. The doping effect of different metal ions including transition metal and rare earth have been studied for its potential application in ultraviolet luminescence devices, light emitting diodes, gas sensors and transparent thin film transistors [93-94]. The ZnO nanoparticles exhibits luminescence in visible region with excitation carried out at different ultraviolet wavelength. Transition metal doping enhances the optical absorption of ZnO. The change in the band gap makes the semiconductor more effective photo catalyst. The Co doped ZnO nanoparticles emerged as one of the most prospective material in spintronic devices due to its RTFM behaviour. In addition, the wide band gap of ZnO and high solubility limit of cobalt in ZnO with large magnetic moment per Co ion make it an ideal material for short wave magneto-optical devices. The important feature of TM doped ZnO nanoparticles are that its properties can be easily tailored as per the demand of device fabrication.

The experimental results of magnetic property in Co doped ZnO are quite controversial, giving rise to ferromagnetism or paramagnetic behaviour depending upon the preparation condition [95-96]. Ferromagnetism in Co doped ZnO has been reported by

different authors [97]. *F. Ahmed et al.* found RTFM in Co doped ZnO prepared by an auto combustion method [37], while *Rao et al.* observed absence of ferromagnetism in Co doped ZnO [38]. The existence of ferromagnetic ordering in Co doped ZnO has been theoretically proposed, which is attribute to the double exchange interaction between Co ions [98]. Latter, ferromagnetism is also explained by Ruderman-Kittel-Kasuya- Yosida (RKKY) interaction [99]. The formation of Co metal cluster has been also considered to explain RTFM. However, the basic mechanism of RTFM in Co doped ZnO is still a topic of discussion and correlation between magnetic and optical properties is not completely clear due to contradictory results in the literature. These controversial results indicate that RTFM in DMS is extremely sensitive to preparation methods. In case of DMS, the type of carriers, their mobility and density give a chance to control their magnetic properties.

ZnO can absorb UV light. As we know that visible light contains highest percentage (45%) of solar spectrum, so in order to improve absorption properties for better photo catalytic activity and other applications, ZnO should have ability to absorb both UV and visible light. For this, band gap of ZnO has to be narrowed or to be split up in to several sub band gaps; this can be achieved by incorporation of transition metal ions such as Mn, Fe, Co and Ni. The small lattice defect or disorder introduced in the host semiconductor due to substitution of transition metal ions are also responsible for change in structural, optical and magnetic properties of host semiconductor. The DMS provides a possibility of energy band gap tuning by changing the doping concentration. This band gap engineering through transition metal doping firmly empowers the investigation of the magneto optical properties of the transition metal doped ZnO system. This may prompt the advancement of the novel magneto-optics devices.

In this chapter, we have investigated effect of different Co concentration on structural, optical absorption, emission and ferromagnetic properties of ZnO nanoparticles in order to shed more light on correlation between structural, magnetic and optical behaviour of Co doped ZnO nanoparticles. We have prepared $Zn_{1-x}Co_xO$ (x = 0.00, 0.02, 0.04 and 0.06) nanoparticles with a simple sol gel method and focussed to maintain the hexagonal wurtzite crystal structure of all the samples. This chapter describes the absorption edge shift in visible region, emission peak shift, RTFM in the prepared samples and correlation between magnetic and optical properties using an easier rout of synthesis.

3.2. EXPERIMENTAL PROCEDURE

3.2.1 Synthesis of ZnO: Co Nanoparticles

We have prepared $Zn_{1-x}Co_xO$ (x = 0.00, 0.02, 0.04 and 0.06) samples by sol-gel method. Zinc acetate dehydrate [Zn $(CH_3CO_2)_2.2H_2O$], cobalt acetate tetra hydrate [Co $(CH_3CO_2)_2.4H_2O$] and isopropyl alcohol has been taken as starting materials without any further purifications. For the synthesis of the nanostructure Co2% doped ZnO, we dissolved stoichiometric amount of zinc acetate dehydrate in isopropyl alcohol with the help of magnetic stirring for 1h and then added stoichiometric amount of cobalt acetate tetra hydrate with stirring 1h for complete dissolution of the precursors. Urea has been added for proper burning of samples and string continued 4h for gel preparation. We have maintained the temperature and rpm at 80^oC and 1200 rpm respectively during gel formation. The resultant gel undergoes burning at 500^oC for 30min followed by sintering at 600^oC for 2h in pellet form. All the samples have been prepared with the same synthesis process. All the characterisations have been done in powder form (obtain by crushing the pellets). Only energy-dispersive x-ray spectroscopy (EDS) analysis has been done in pellet form with gold coating on pellets.

3.2.2 Characterisations

We have confirmed proper phase confirmation of synthesized samples using Rigaku-MiniFlex-II DESKTOP powder X-ray diffractometer with CuK_{α} radiation (λ= 1.54 Å) at 30kV and 15mA. All patterns were recorded over the range $20^{o} \leq 2\theta \leq 80^{o}$ with a step size of 0.02º. The morphology and particle size have been investigated with TECNAI G^2 200kV TEM (FEI) Transmission Electron Microscope (TEM). OXFORD Instrument SEM EVO 18 Research has been used for EDS analysis to confirms presence of all elements in the samples. The optical absorption spectra of the samples were recorded by the Lambda–35 UV-Vis spectrophotometer from PerkinElmer in the range of 200-800nm. Photoluminescence spectra have been recorded by Horiba Fluorolog-3 spectrophotometer equipped with 450w Xe flash lamp. Fourier Transform Infrared (FTIR-8400S) spectrophotometer has been used to obtain information about functional groups present in the samples. The magnetic behaviour has been investigated using Quantum Design MPMS-3 magnetometer in temperature range 5-300 K.

3.3. RESULTS AND DISCUSSIONS

3.3.1 Structural Analysis

Figure 3.1 depicts the XRD spectra of $Zn_{1-x}Co_xO$ (x = 0.00, 0.02, 0.04 and 0.06) nanoparticles sintered at 600°C. The XRD pattern shows that intensity of peak is narrow, which indicates that samples are highly crystallite. All the peaks are properly indexed according to hexagonal wurtzite crystal structure of pure ZnO nanoparticles (PDF: 792205). All the samples have single phase without any impurity phase within the detection limit of instrument. The XRD results indicate that cobalt behaves as a substitutional dopant in ZnO without changing the wurtzite crystal structure. The lattice constants (*a* and *c*) of Co doped ZnO has been calculated with unit cell software and listed in Table 3.1. For HCP structure $a = b \neq c$ and c/a =1.633.

In our observation the lattice parameters *a* and *c* shows a little random change with Co concentration but both *a* and *c* have same behaviour (when *a* increases *c* also increases and same nature for decrement). The lattice parameter ratio *c/a* is 1.60 and shows small change at third/forth decimal point. This change in lattice parameter value with Co concentration may be due to ionic radius mismatch between zinc (0.60Å) and cobalt (0.58Å)[100].

Table 3.1: Lattice parameter and crystallite size of Co doped ZnO.

Co %	a(Å)	c(Å)	c/a	Cell volume	Crystallite size (nm)
0	3.25015	5.20469	1.601369	47.6138	36.2
2	3.24787	5.20118	1.601412	47.515	28.5
4	3.25113	5.2102	1.602581	47.693	32.6
6	3.24805	5.19974	1.60088	47.5069	34.1

The XRD analysis confirms that all samples possess hexagonal wurtzite structure with space group $P6_3mc$. The variation in lattice parameter confirms the substitution of Co ions in Zn site of ZnO crystal structure. The crystalline size of $Zn_{1-x}Co_xO$ (x = 0.00, 0.02, 0.04 and 0.06) have been calculated using Scherer's formula[101]

$$D = \frac{0.9\lambda}{\beta cos\theta} \qquad \ldots\ldots\ldots\ldots \quad (3.1)$$

Where λ is wavelength of X- rays (1.54 for Cu K_α), θ is Bragg's angles & β is the full width at the half maximum.

The crystalline quality of the samples remains unchanged because Co ions incorporated in to Zn site of ZnO crystal structure rather than interstitial ones [102]. The values of crystalline size are listed in Table 3.1. It has been observed that crystalline size is initially decreases due to Co2% doping and then increases with cobalt concentration. It may be due to fact that, for Co2% the lattice easily accepts the Co ions without affecting ZnO

structure. The similar pattern of crystalline size variation has been observed by *R. Ponnusamy et al.*[103]. The change in crystalline size depends on growth of ZnO grains. The growth of ZnO grains are affected by movement and diffusion of Zn^{+2} ions. However, in case of cobalt doped ZnO, Co may exist as the grain boundary which enhance the energy barrier of the movement, the diffusion of Zn^{+2} and increase the electrical resistivity, therefore restrain the grain growth of ZnO grains[104]. The cobalt act as electrical doping for small doping concentration, when doping percentage increases, impurity also increases which increase the electrical conductivity because it can diffuse. Thus the grain size increases with Co concentration from 2- 6%.

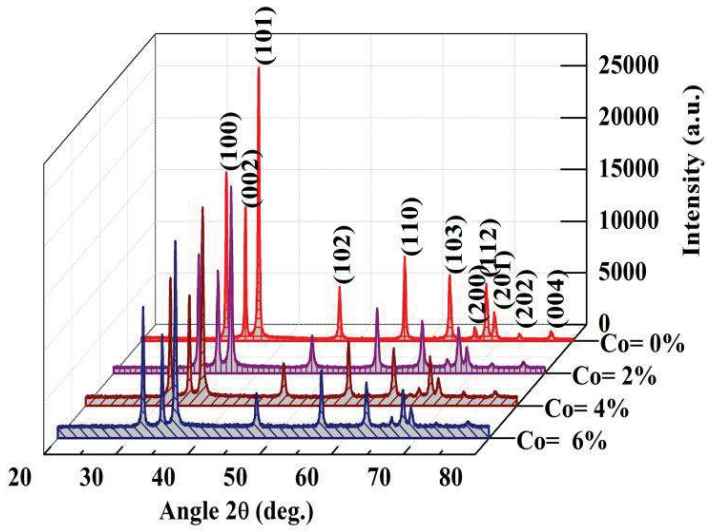

Figure 3.1: XRD pattern of $Zn_{1-x}Co_xO$ nanoparticles.

3.3.2 Morphology and Elemental Analysis

The morphological analysis of the samples has been done with the help of TEM shown in Figure 3.2(a) and 3.3(a) for ZnO and Co2% doped ZnO respectively. The TEM micrographs indicates that most nanoparticles are more or less spherical in shape and smooth in surface having the distribution of size between 10-70 nm with average particles size 42.8 nm for Co doped ZnO and 68.6 nm for pure ZnO nanoparticles. The average particle size of these nanoparticles were estimated by considering the minimum

and maximum diameter of large number of particles. The particle size distribution for ZnO and Co2% doped ZnO are shown in Figure 3.2(d) and 3.3(d). The SAED pattern for ZnO and Co2% doped ZnO are shown in Figure 3.2(b) and 3.3(b). The ring pattern confirms the polycrystalline nature of samples. The SAED pattern of single particle of Co doped ZnO is shown in Figure 3.3(e). The diffraction pattern clearly shows that crystal has hexagonal structure. Thus we can say that all the samples have hexagonal crystal structure. The average particle size of Co2% doped ZnO is less than pure ZnO nanoparticles. The variation in particles size and presence of hexagonal crystal structure obtained by TEM analysis support the XRD results.

Energy dispersive X-ray spectroscopy has been used for qualitative and quantitative analysis of the entire element present in the samples. The EDS pattern has been shown in Figure 3.2(c) and Figure 3.3(c) for ZnO and Co doped ZnO nanoparticles. The peaks observed in EDS confirm the presence of Co and Zn over the selected scan area of samples. The same process has been used for all the samples under investigation. The ratio of Zn: Co: O has been given in Table 3.2, which confirms the presence of Cobalt in ZnO structure. It has been observed that atomic and weight percentage of Co within the scanned area increases with increase in doping concentration. The increase in weight percentage of Co within the scanned area has good agreement with doping percentage.

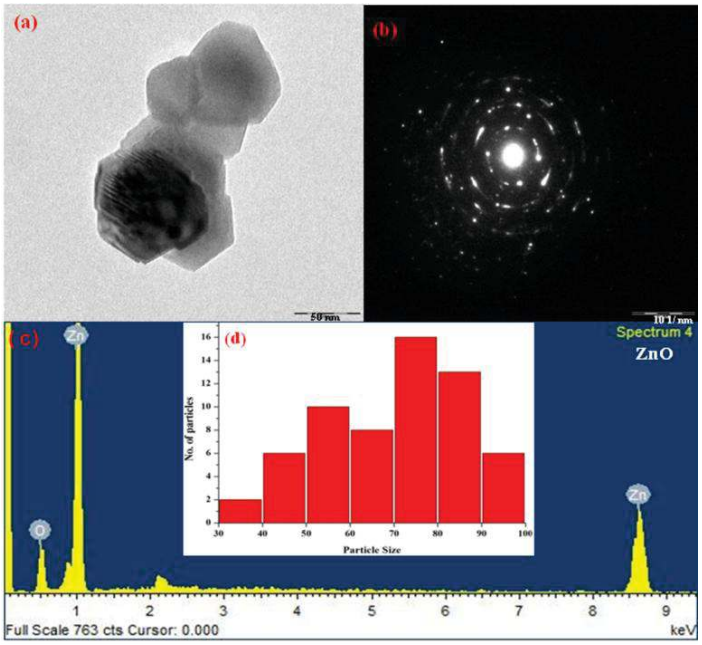

Figure 3.2 (a) TEM image, **(b)** SAED pattern **(c)** EDS spectra **(d)** particle size distribution of ZnO nanoparticles.

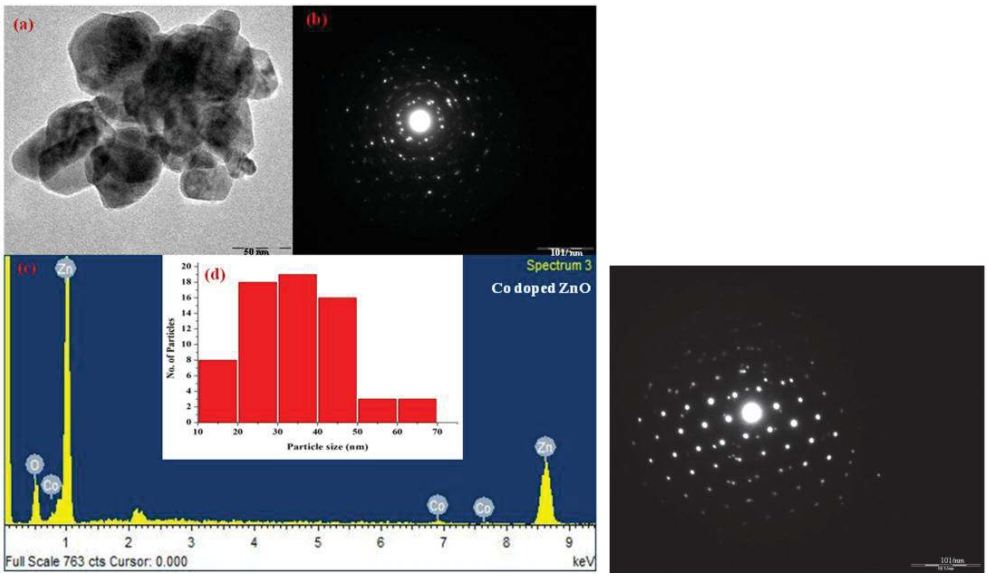

Figure 3.3 (a) TEM image, **(b)** SAED pattern **(c)** EDS spectra **(d)** particle size distribution of Co 2% doped ZnO **(e)** SAED pattern of single particles of Co 2% doped ZnO.

Table 3.2: Data for atomic and weight percentage of all the samples.						
Co %	Zn		Co		O	
	Atomic %	Weight %	Atomic %	Weight %	Atomic %	Weight %
0	52.86	82.08	0	0	47.14	17.92
2	48.97	79.02	0.77	1.13	50.26	19.85
4	47.60	76.66	2.54	3.68	49.87	19.66
6	50.82	78.04	3.45	4.78	45.72	17.18

3.3.3 FTIR Studies

Figure 3.4 shows FTIR spectroscopy of the synthesized pure and Co doped ZnO nanoparticles within the range of 450- 4000 cm^{-1}. The FTIR analysis has been performed to study the functional group present in the samples, inter or intra molecular interactions, the vibrational band due to Zn-O bonds and the change due to Co incorporation in ZnO. Table 3.3 represent the assignment of the peaks observed in $Zn_{1-x}Co_xO$ (x = 0.00, 0.02, 0.04 and 0.06) nanoparticles. It has been observed that all the prominent peaks of ZnO are also present in Co doped ZnO nanoparticles. The small shift in the peak positions indicate small lattice distortion but crystal structure is maintained in all the samples under investigation. The analysis of FTIR spectra has been done based on the results published in the literatures [35, 100,103]. The absorption peaks of all the samples in the range of 400- 700 cm^{-1} can be attributed to Zn-O stretching modes [105]. The strong absorption band at 588 cm^{-1} is due to Zn-O stretching modes, which confirms the formation of ZnO nanoparticles [103]. Zn-O stretching mode has a blue shift from 588 cm^{-1} to 603 cm^{-1} with increase in Co concentration. The blue shift observed in the sample is due to atomic mass difference between Zn and Co ions. Since Co (58.93u) has less atomic mass as compared to Zn (65.38u), therefore Co must have vibrational modes in the higher wave

number region. The weak vibration of ZnO is observed at wave number 872 cm^{-1}. All the observed absorption peaks for O-H and C=O are also assigned and tabulated in Table 3.3. Thus the result of XRD, TEM and FTIR authenticates the substitution of cobalt and hexagonal crystal structure formation of all the samples under investigation.

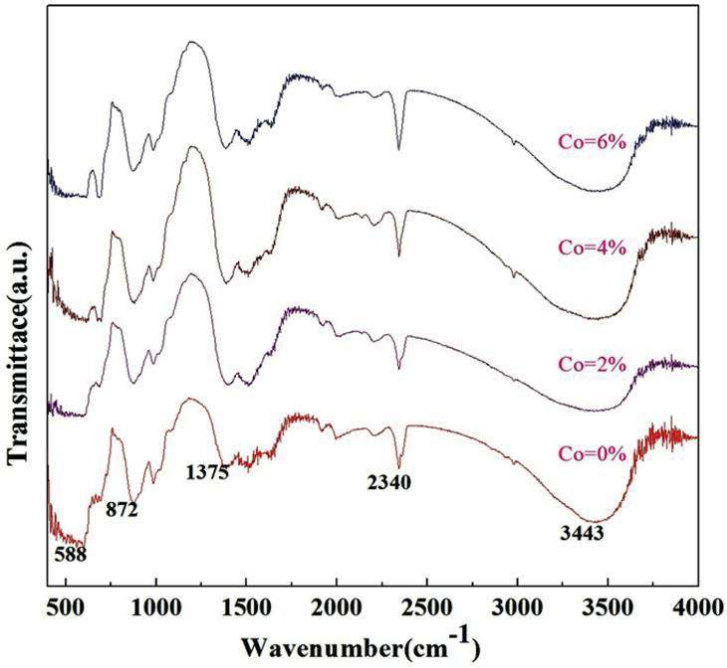

Figure 3.4: FTIR spectra of $Zn_{1-x}Co_xO$ nanoparticles.

Table 3.3: FTIR peak assignment of samples.

Wave numbers (cm^{-1})				Assignments
ZnO	$Zn_{0.98}Co_{0.02}O$	$Zn_{0.96}Co_{0.04}O$	$Zn_{0.94}Co_{0.06}O$	
588, 686	592, 684	603, 686	603, 684	Zn-O stretching
872	875	873	877	Weak vibration of ZnO
1001	981	981	981	O-H asymmetric stretching
1375	1394	1396	1379	Symmetric stretching of C=O
1505	1518	1502	1506	Asymmetric stretching of C=O
2340	2340	2336	2336	Co_2 molecule in Air
3443	3458	3428	3453	O-H stretching

3.3.4 UV-Vis Spectroscopy

UV-Vis analysis has been done to investigate the effect of Co doping on the absorption and band gap of samples. The absorption spectra has been recorded within the range of 200-800 nm and shown in Figure 3.5. It has been observed that increase in cobalt concentration results encroachment in visible region with red shift in band edge. In case of Co doped ZnO, three additional peaks has been observed at 655, 610 and 565 nm. The visible region absorption increases with Co concentration. These visible region absorption peaks can be attributed to *d-d* transition of tetrahedral coordinates Co^{+2} ions in ZnO hexagonal wurtzite crystal structure and correlated with $^4A_2(^4F) \rightarrow {}^2E(^2G)$, $^4A_2(^4F) \rightarrow {}^4T_1(^4P)$ and $^4A_2(^4F) \rightarrow {}^4A_1(^4G)$ transitions[106-107]. The presence of additional peaks confirms the Co incorporation in the ZnO host lattice.

The band gap of samples under investigation have been determined by applying the Tauc relationship[104] as given below-

$$\alpha h\nu = B(h\nu - Eg)^n \quad \ldots\ldots\ldots\ldots \qquad (3.2)$$

Where α is absorption coefficient given by $\alpha = {}^{-A}/_{d}$ (d is the thickness of sample cell and A is the absorbance), *hν* is photon energy, B is a constant and E_g is the energy band gap of the material. The value of '*n*' depends on the type of the transitions. *n* = 1/2, 2, 3/2 for allowed, indirect and forbidden transition respectively. The band gap has been calculated by extrapolation of linear part that meets the abscissa in plot of $(\alpha h\nu)^2$ versus photon energy *(hν)* as shown in Figure 3.6(a). The same pattern has been followed for calculating band gap of other samples. The variation of band gap with Co percentage has been shown in Figure 3.6(b). It has been observed that band gap decreases with Co concentration and varies between 3.2-3.0eV. This red shift in the band gap energy can be attributed to sp-d exchange interaction between ZnO band and electrons and localised *d* electron (moments) of doped Co ions. The magnetic behaviour of samples also affects the

band gap of materials. The red shift in the band gap of DMS has been observed by some authors [108-109]. The ferromagnetism in cobalt doped ZnO is due to localized magnetic moments mediated by free charge carriers. It has been observed that magnetic behaviour increases with Co concentrations; this indicates increase in the charge carriers with Co doping this increase in charge carriers affects the sp-d exchange interactions by increasing *d* electron moments of Co ions, which could results the red shift in the band gap.

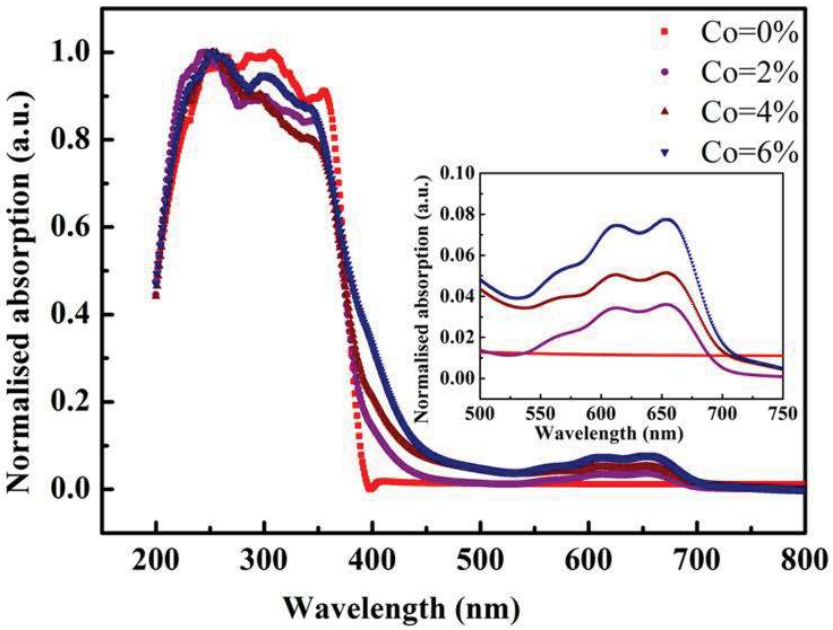

Figure 3.5: Absorption spectra of $Zn_{1-x}Co_xO$ nanoparticles.

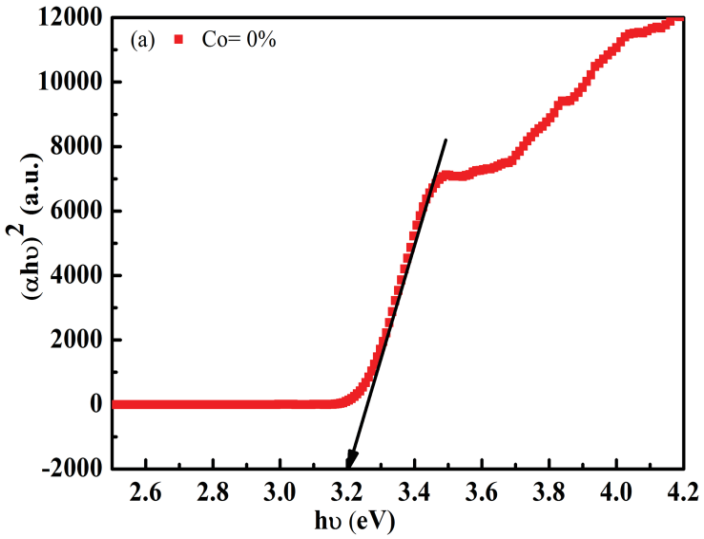

Figure 3.6(a): $(\alpha h\nu)^2$ versus photon energy of ZnO nanoparticles.

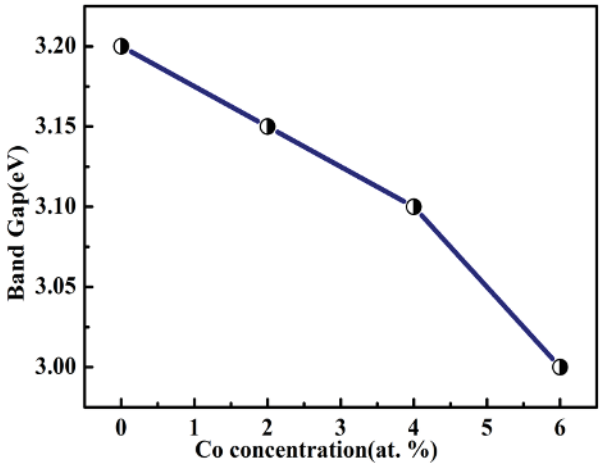

Figure 3.6(b): Energy band gap versus Co concentration of $Zn_{1-x}Co_xO$.

3.3.5 Photoluminescence Spectroscopy

The photoluminescence (PL) spectra of Co doped ZnO nanoparticles with different doping concentration have been recorded at room temperature. Figure 3.7 (a) and (b) shows PL spectra and chromaticity diagram of all the samples under investigation. ZnO has emission in visible region with prominent peak in violet colour (436 nm), while cobalt doped ZnO samples have intense peaks at 467nm (blue colour). This result indicates that Co doping shift the intense peak position of ZnO from violet to blue colour. The weak emission peak at 572 nm also observed in all the samples. The peak position of $Zn_{1-x}Co_xO$ (x = 0.00, 0.02, 0.04 and 0.06) observed at 400, 398,396 and 398 nm respectively can be attributed to near band edge emission (NBE) originating from the recombination of excited electron from a localised level below the conduction band with the hole in valence band [110]. The intensity of these peaks decreases with Co contents, which indicates that crystal quality decreases due to Co doping. The small lattice distortion is due to ionic radius mismatch between Co and Zn ions. *Antony et al.* observed that UV emission disappeared in Co doped ZnO nanocluster [111]. The violet band centred at 436 nm can be attributed to electron transition from shallow donor level (Zn_i) to valence band [110]. The violet blue and blue emission around 436 and 467 nm

may also be due to defect related positively charge Zn vacancies[112]. The weak intensity green emission at 572 nm can be attributed to recombination of electron with hole trapped in singly ionised oxygen vacancies [113]. Figure 3.7(b) shows the 1931 CIE chromaticity diagram of all the samples under investigation with excitation wavelength 320 nm. The observed colour coordinate for $Zn_{1-x}Co_xO$ (x = 0.00, 0.02, 0.04 and 0.06) samples are (0.20, 0.23), (0.02, 0.24), 0.23, 0.28) and (0.21, 0.27) respectively. From the colour coordinate demonstration in Figure 3.7(b) it is clear that emission is in the blue area.

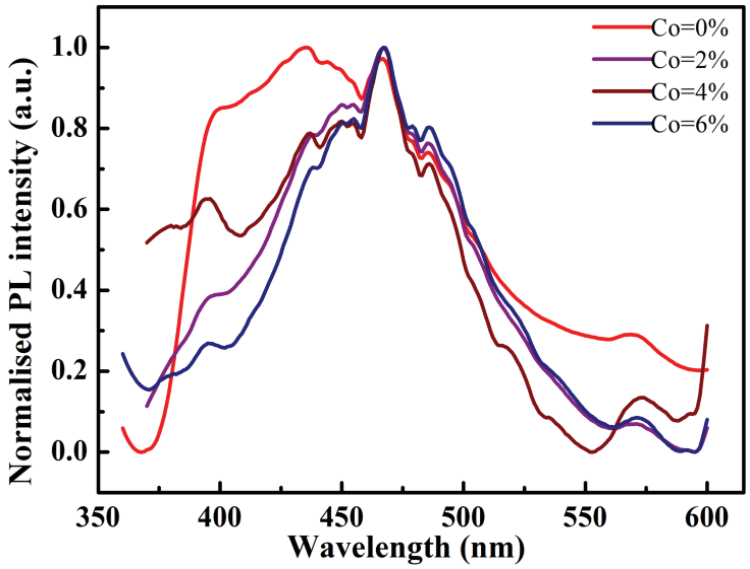

Figure 3.7(a): Photoluminescence spectra of $Zn_{1-x}Co_xO$ nanoparticles.

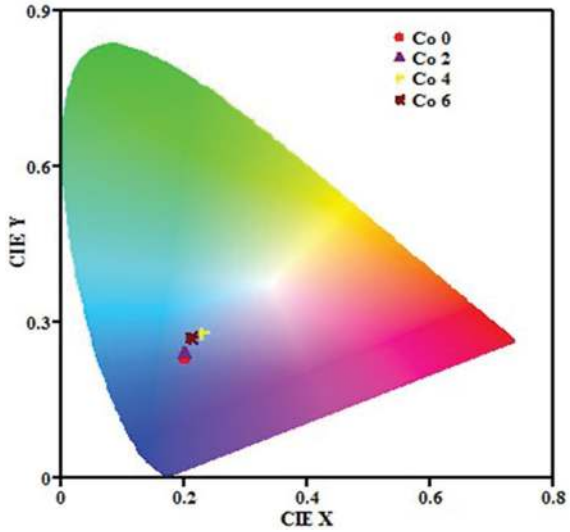

Figure 3.7(b): CIE diagram of $Zn_{1-x}Co_xO$ nanoparticles.

3.3.6 Magnetic Properties

The vibrating sample measurement (VSM) system has been used to know the information about magnetic properties of $Zn_{1-x}Co_xO$ (x=0.00, 0.02, 0.04 and 0.06) nanoparticles. The variation of magnetization versus magnetic field measured at 300K with maximum applied field of ±1.5 T for different Co concentration has been plotted in Figure 3.8. Figure 3.9 (a) represents a close scan near the origin for pure ZnO nanoparticles. The plot shown in Figure 3.8 indicates that an increase of Co concentration increases the linear behaviour of M-H loop. It implies that higher Co concentration favoured the Co-Co exchange at room temperature. The coercive field (H_c) and the remanent magnetisation (M_r) increases with Co doping concentration. The increase in M_r value indicates that the material can sustain magnetisation. The values of M_r and H_c are summarised in Table 3.4. Transition metal (Mn, Co, and Fe) doped ZnO based DMS have number of potential application in spintronic devices such as spin polarised LED's and spin transistor [114]. The magnetic atoms of this type of semiconductor substituted at cationic site of the host materials. The ferromagnetism in DMS has been explained on the basis of diversity of theories such as super exchange, indirect exchange, Ruderman- Kittel Kasuya- Yosida (RKKY) interaction[99] free carrier mediated exchange, sp-d exchange mechanism [115] and double exchange between the *d* states of the transition metals [98]. The sp-d exchange interaction involve the strong interaction between localised *d*- type electron of transition metal ions and the localised *s* or *p* band electron present in Zn or oxygen atom [116]. The RTFM in Co doped ZnO have quite controversial experimental results. In addition to magnetic doping effect, oxygen vacancies defect have been suggested the reason of RTFM origin for oxide DMS [114]. In this work, we have observed that anti ferromagnetic coupling are also present between transition metal atoms in Co doped ZnO. The distance between Co ions decreases with increase in Co

concentration, this lead to anti ferromagnetic exchange. The temperature dependent susceptibility plots for different Co concentration have been shown in Figure 3.10. It has been observed that susceptibility decreases with temperature. An abrupt decrease in susceptibility value can be associated magnetic phase change. We have observed that ZFC-FC plots for each sample does not show any significant difference i.e. ZFC-FC data lies approximately on the same point in the curve. Figure 3.9(b) represent ZFC-FC plot of pure ZnO nanoparticles. All the samples exhibit curie wises behaviour. The curve of $1/\chi$ versus T has been used to calculate the Curie temperature. The calculated Curie temperature for $Zn_{1-x}Co_xO$ (x = 0.00, 0.02, 0.04 and 0.06) are 693, 125, 91 and 75 K respectively. In light of the above discussion, the existence of ferromagnetism in our case can be explained as follows. The XRD result indicates that all the samples are single phase. The presence of secondary phase of cobalt oxides like CoO_2, Co_3O_4 and $ZnCoO_4$ are not observed within the detection limit of instrument. However, lattice distortion take place due to Co incorporation in ZnO nanopowder. Therefore, we believe that RTFM in our samples is due to defect and incorporation of Co ions in ZnO host. The relation between structural defect and RTFM has been discussed with different authors. Thus our study also suggests that defect is an important factor affecting the magnetic properties of Co doped ZnO.

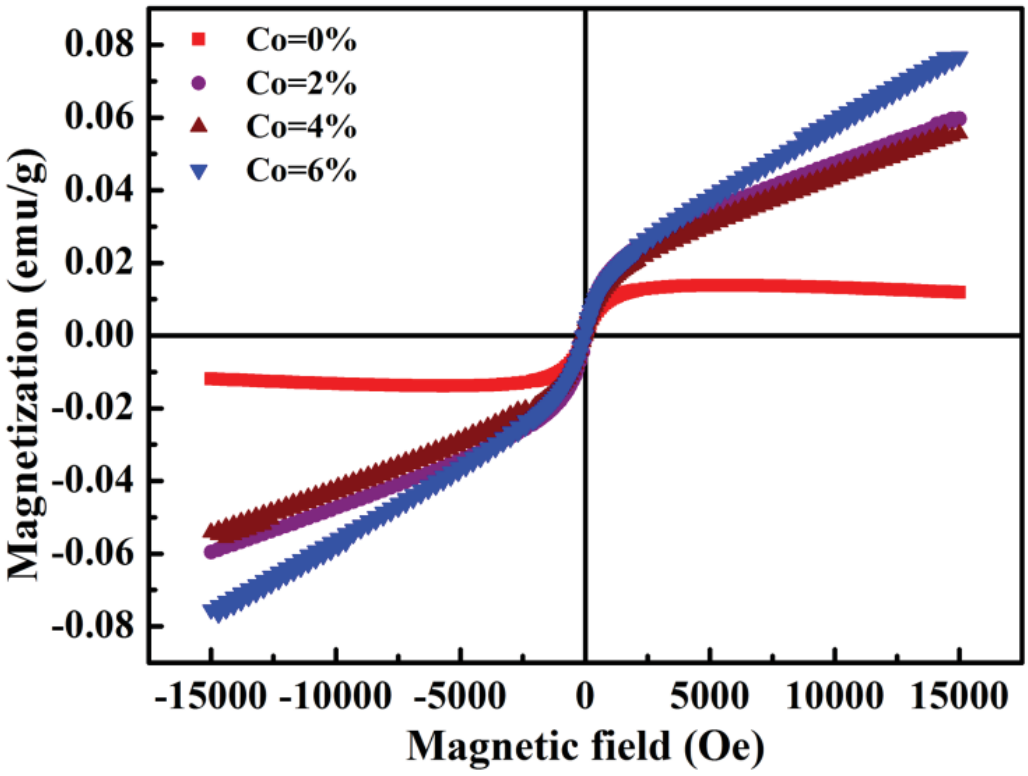

Figure 3.8: M-H curve of pure and Co doped ZnO nanoparticles at 300 K.

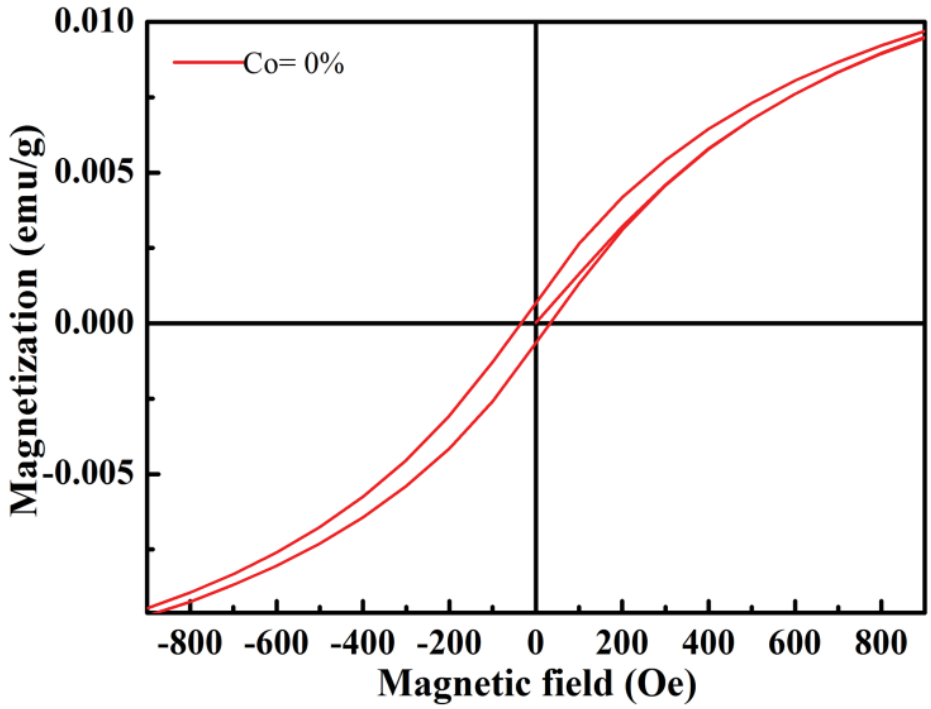

Figure 3.9(a): M-H curve of pure ZnO nanopowder at 300 K

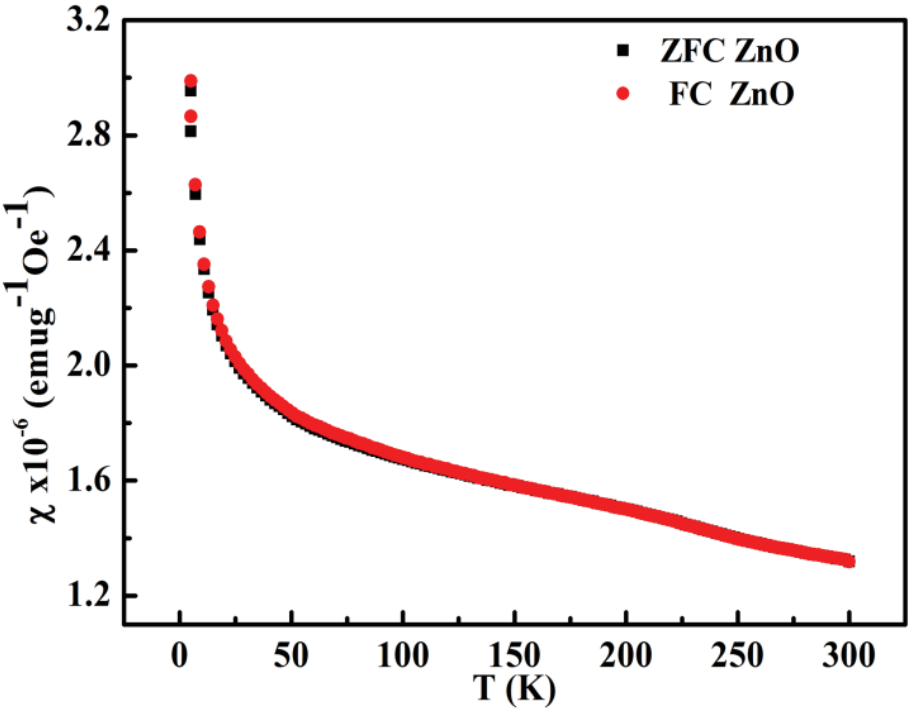

Figure 3.9(b): Susceptibility curve (ZFC-FC) of pure ZnO.

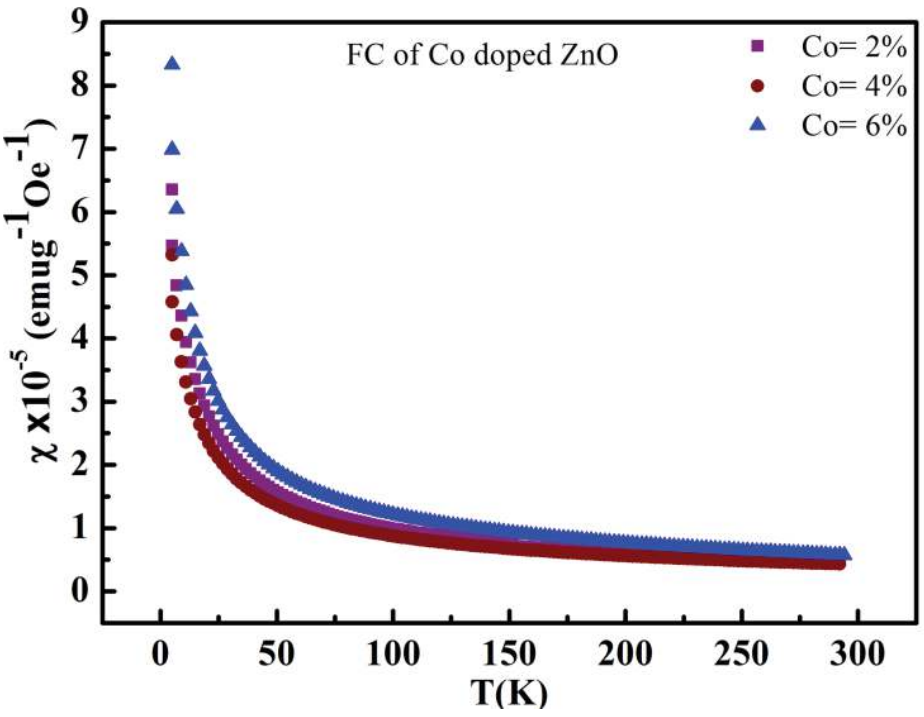

Figure 3.10: Susceptibility curve of Co doped ZnO.

Table 3.4: Variation in H_c, M_r, and T_c values.			
Co (at %)	H_c(Oe)	M_r(emu/g)	T_c(K)
0	35.05	0.000728	693.01
2	40.67	0.001296	125.38
4	66.63	0.001571	91.86
6	37.77	0.001206	75.02

3.4. CONCLUSION

In this study, we have observed the modification in structural, optical and magnetic properties of ZnO nanoparticles with different Co concentration. The analysis confirms that Co incorporation significantly affect the structural, absorption, emission and magnetic properties of ZnO nanoparticles. The results of XRD, EDS, TEM and FTIR demonstrate the formation of single phase hexagonal wurtzite crystal structure of all the samples under investigation. The absorption study indicates that increase in Co concentration improves the visible light absorption (550-700 nm) and encroachment of band edge in visible region. The increase in Co concentration result a red shift in band gap of samples. The emission properties measured with the help of photoluminescence spectroscopy implies that the prominent peak position of ZnO nanoparticles shift from violet to blue colour due to Co doping. Some weak emission peak at 572 nm is also present in the samples. The magnetic result suggests that small lattice defect can affect the RTFM. The increase in H_c and M_r values indicate an increase in RTFM of Samples.